Magnetic Resonance Imaging 61 (2019) 167–174

Contents lists available at ScienceDirect

Magnetic Resonance Imaging

journal homepage: www.elsevier.com/locate/mri

Original contribution

Computation of the resonance frequencies of the transmission line resonators used in MRI

Alex Protopopov[a,b], Mikhail V. Gulyaev[c,*], Olga S. Pavlova[c,d], Elizaveta A. Mokhova[d], Yury A. Pirogov[d,e]

[a] Department of Medical and Biological Physics, Moscow Institute of Physics and Technology, 141701 Moscow Region, Dolgoprudniy, Institutskiy per., 9, Russia
[b] Federal Scientific Clinical Center for Gematology, Oncology, and Immunology, 117997 Moscow, GSP-7, Samora Mashel str., 1, Russia
[c] Faculty of Fundamental Medicine, Lomonosov Moscow State University, 117192 Moscow, Lomonosovsky Prospekt, 31-5, Russia
[d] Faculty of Physics, Lomonosov Moscow State University, 119991 Moscow, GSP-1, Leninskie Gory, 1-2, Russia
[e] Institute of Engineering Physics for Biomedicine, National Research Nuclear University MEPhI, 115409 Moscow, Kashirskoe shosse, 31, Russia

ARTICLE INFO

Keywords:
Transmission line resonators
Resonance frequency computation
Single-nucleus MRI

ABSTRACT

Stripline high frequency resonators or transmission line resonators (TLRs) manufactured as concentric RF coils at the opposite sides of a dielectric sheet serve as wireless self-resonant transmitters-receivers in MRI. Owing to their high quality factor relative to traditional RF coils composed of bulk inductor and capacitors, frequency selectivity of TLRs is high, making them promising elements for single-nucleus MRI. However, the computation of their resonance frequencies is cumbersome, and numerous mathematical mistakes and typos in publications lead to incorrect results. The present publication is the first to summarize the corrected formulas for computations and presents comparison of such computations to real measurements.

1. Introduction

Single-nucleus magnetic resonance imaging (MRI) requires the use of radiofrequency (RF) coils with high frequency selectivity that is determined by the quality factor, or Q factor, of the RF coil [1]. The quality factor Q, in turn, is determined by losses in resonating circuit and by absorption in the surrounding medium. When a standard, not isolated RF coil composed of bulk inductance and capacitors is placed over a patient body, the body tissues behave as a dielectric layer inside the virtual capacitor between the coil and the ground, leading to additional dielectric losses and a decrease of Q. It could be possible to solve this problem only if the body is isolated from the RF coil. However, it is impractical due to design limitations.

Zabel et al. [2] proposed an elegant solution to this problem, using coaxial line resonator with short circuit at its end. In this case, dielectric losses in the body of a patient decrease, since displacement currents, created by the central wire, are shielded by grounded braids. This feature allowed increased frequency selectivity of the coil. This idea soon evolved into a new type of the RF coils in MRI - resonant transmission line coils or transmission line resonators (TLRs), which are under discussion in the present work.

Another advantage of such coils is their simple and compact design, which makes them available for virtually any resonance frequency and size. However, computation of the resonance frequency for a specific design typically requires complex and time-consuming simulations. Formulas for approximate computation of the resonance frequencies have been proposed in earlier papers [3–7], but contained numerous misprints and errors, making them hard to implement. The current work presents corrected version of these formulas, and tests them in practice on several TLRs.

2. Theory

2.1. Transmission line resonator

It is well known that a transmission line, such as a coaxial cable, for instance, displays resonant performance when it is short-circuited (Fig. 1). Its input impedance Z is at maximum and equals infinity when the length of the line l is equal to the quarter of the wavelength [8]. Due to electromagnetic field being localized entirely inside the shield, such a line does not radiate.

Now, consider such a resonator turned into a loop (Fig. 2a). Since currents along the central wire (I_w) and the shield (I_{sh}) are equal to each other and directed oppositely, such a loop neither produces an external magnetic field, nor does the external magnetic field induce a current in the central wire. But if the shield is disrupted (Fig. 2b), the magnetic

* Corresponding author.
E-mail addresses: gulyaev@physics.msu.ru (M.V. Gulyaev), mokhova.ea15@physics.msu.ru (E.A. Mokhova).

https://doi.org/10.1016/j.mri.2019.05.002
Received 3 February 2019; Received in revised form 1 May 2019; Accepted 2 May 2019

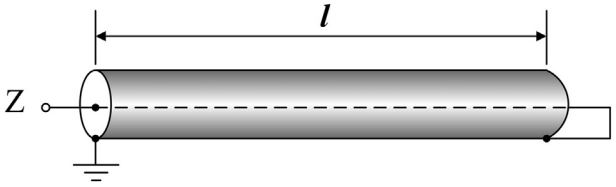

Fig. 1. Short-circuited coaxial cable.

fields induced by the shield and central wire do not compensate each other anymore, and such a loop works both as a transmitter and a receiver of magnetic field.

Better technological flexibility and reproducibility in manufacturing may be achieved with ring resonators formed by circular striplines placed on both sides of a dielectric - like printed circuit boards (Fig. 3). The dielectric may be either fiberglass or polyimide film.

Such resonators are also named TLRs. In the paper of Frass-Kriegl et al. [6] the main types of them were presented. In this paper, we are demonstrated them in Fig. 4.

Among the TLRs, the MTMG-TLRs (Multi-turn multi-gap transmission line resonators) are of particular interest because of a large set of parameters that can be changed for obtaining a different resonance frequency: outer coil diameter, turn radii, width of the conducting strips, width of the spaces between the turns, number of turns, number of gaps, thickness of the dielectric, dielectric permittivity [6].

2.2. Mathematical form of the problem

The key factor in designing the TLRs is the computation of its resonance frequency f_0, at which the produced magnetic field is at a maximum. Such an attempt was first undertaken by Gonord et al. [3], considering the stripline resonator shown in Fig. 3. Within the equivalent circuit of dubious applicability, the formula for the computation of $\omega_0 = 2\pi f_0$ was obtained as an equation with the parameters being the inductance of a single coil L, characteristic impedance of the stripline Z_0, and lengths l_1 and l_2 of the left and right parts of the split bottom layer of the coil, counting from the grounding point (Eq. (1) in [3]).

However, that formula produced lower values of the resonance frequency ω_0 than expected. Therefore, in their next publication, the same authors developed a different theory for the condition of resonance [4]. According to it, the resonance occurs not when the impedance tends to infinity, as they suggested originally in [3], but when all the partial currents in both the upper and lower strip sections are in the same direction. If such a condition exists, then, evidently, the magnetic field in the center of the coil will maximize since both the lower and upper coils generate magnetic field in the same direction at the center of the coil. Regretfully, even with this better model generalized to n symmetrical gaps in each strip (total $2n$ gaps), the authors gave an incorrect formula again (Eq. (20) in [4]).

The mistake was identified later by Serfaty et al. [5] and announced in a footnote on the very first page. However, inexplicably, the footnote itself and the final formula (Eq. (1) in [5]) were both given with errors.

Eventually, the errors were weeded out over the course of multiple publications until a correct formula was finally given by Frass-Kriegl et al. [6] in the following way (Eq. (1) in [6]):

$$\frac{\omega_0 L}{4nZ_0}\cdot\tan\frac{\omega_0 l\sqrt{\varepsilon}}{4nc} = 1 \tag{1}$$

In Eq. (1) ω_0 is the resonance frequency of the coil, L and Z_0 – the coil's inductivity and impedance, respectively, n – the number of gaps in the stripline on one side of the coil, l – the total length of loops on one side of the coil, ε – the dielectric permittivity and c – the speed of light. The Eq. (1) was also published by Megherbi et al. [7]. Regretfully, in that work a series of other mistakes marred credibility: in the formulas for resonance condition and characteristic impedance Z_0, and some other discrepancies that will be outlined in the next sections.

2.3. Computation of the resonance frequency

Today, analytical formulas for characteristic impedance of a stripline are available only for the case of a straight isolated stripline, whereas in our case the striplines have a curved shape and cannot be considered exactly isolated, being surrounded by the adjacent turns. Nonetheless, lacking exact analytical solutions for circular striplines, we are bound to use the original Wheeler formulas for straight isolated striplines, having in mind that some obvious corrections should be made in order to compensate for circularity. Original formulas for characteristic impedance Z_0 of a straight isolated line with the strip width w, dielectric permittivity ε and height h are [9]:

$$Z_0 = 120\sqrt{\frac{2}{\varepsilon+1}}\left[\ln\left(\frac{4h}{w}\right) + \frac{1}{8}\left(\frac{w}{h}\right)^2 - \frac{1}{2}\frac{\varepsilon-1}{\varepsilon+1}\left(0.451 + \frac{0.241}{\varepsilon}\right)\right],\ w < h \tag{2}$$

and

$$Z_0 = \frac{120\pi}{\sqrt{\varepsilon}}\left\{\frac{w}{h} + 0.441 + \frac{\varepsilon+1}{2\pi\varepsilon}\left[\ln\left(\frac{w}{h} + 0.94\right) + 1.452\right] + 0.082\frac{\varepsilon-1}{\varepsilon^2}\right\}^{-1},\ w > h \tag{3}$$

The inductance of the coil is computed as the sum of inductances of the upper L_1 and lower L_2 coils and their mutual inductance M_{12} with the following formula:

$$L = L_1 + L_2 + 2M_{12} \tag{4}$$

The inductance of the two flat coils $L_1 = L_2$ is equal to the sum of inductances of each turn they are composed of L_i plus their inter-coil inductance M_{ij}:

$$L_{1,2} = \sum_{i=1}^{N} L_i + 2\sum_{i=1}^{N}\left(\sum_{j>i}^{N} M_{ij}\right) \tag{5}$$

The second sum in this formula is composed only of terms above the diagonal of the matrix M_{ij}.

Now, it is necessary to choose the most accurate formula for computing inductances of each flat turn L_i, because there are a big variety of formulas in the literature, describing various specific peculiarities of coils and their features, leading to numerous different analytical approximations [10]. Such a variety often leads to confusion and use of the formulas that are not applicable to a certain specific case. In particular, Megherbi et al. [7] claims the use of the Coffin formula in the form:

$$L_i = \mu_0 r_i\left(\ln\frac{8r_i}{w} - \frac{1}{2} + \frac{w^2}{96r_i^2}\left[\ln\frac{8r_i}{w} + \frac{43}{12}\right]\right) \tag{6}$$

with $\mu_0 = 4\pi\cdot 10^{-7}$H/m being magnetic constant of vacuum (vacuum permeability). In fact, the Coffin formulas are not applicable to coils confined in a single plane. They were introduced in the beginning of the 20th century as an approximate expansion of inductance of single-layer multi-turn coils into a series over powers of b/r, with the length of the coil b being greater than zero [11]. Identification of the stripline width w with the coil length b is an obvious mistake.

While choosing the proper formula for L_i, it is necessary to realize that even the simplest approximations produce quite good results with a relative error of ~1/500. For instance, the historically first Kirchhoff formula for inductance of a flat turn of radius r_i made by a wire of a

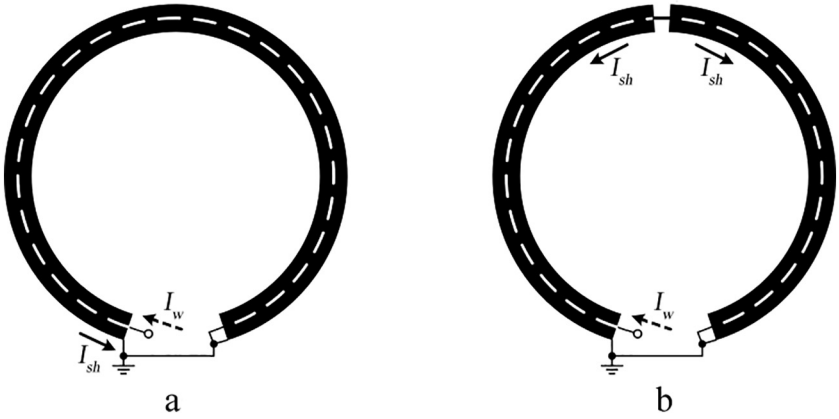

Fig. 2. Coaxial ring resonator. Arrows show direction of currents along the central wire (I_w) and the shield (I_{sh}).

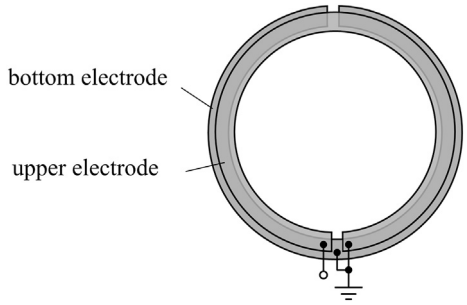

Fig. 3. Circular stripline resonator.

round cross section with the radius a (Eq. (59) in [10]) may be used:

$$L_i = \mu_0 r_i \left(\ln \frac{8r_i}{a} - 1.75 \right) \tag{7}$$

We shall be using the even more accurate Maxwell formula (Eq. (60) in [10]):

$$L_i = \mu_0 r_i \left[\left(1 + \frac{3}{16}\frac{R^2}{r_i^2} \right) \ln \frac{8r_i}{R} - 2 - \frac{1}{16}\frac{R^2}{r_i^2} \right] \tag{8}$$

in which R - the so called geometrical mean distance. It is convenient because it makes it possible to take into account the geometrical shape of the wire, computing R for a given specific shape of its cross section. Namely, for the rectangular lead of the cross section $a \times b$ (Eq. (124) in [10]):

$$\ln R = \ln \sqrt{a^2 + b^2} - \frac{1}{6}\frac{a^2}{b^2} \ln \sqrt{1 + \frac{b^2}{a^2}} - \frac{1}{6}\frac{b^2}{a^2} \ln \sqrt{1 + \frac{a^2}{b^2}} + \frac{2}{3}\frac{a}{b} \operatorname{arctg} \frac{b}{a} + \frac{2}{3}\frac{b}{a} \operatorname{arctg} \frac{a}{b} - \frac{25}{12} \tag{9}$$

This symmetrical formula can be easily simplified for an infinitely thin lead with $b \to 0$, which is the case of a copper layer on a printed-circuit board. The result, computed in the Appendix, is as follows:

$$R = a \cdot e^{-3/2} \approx 0.223a \tag{10}$$

As a result, substituting a for w, the Eq. (8) takes the form:

$$L_i = \mu_0 r_i \left[\left(1 + 0.0093\frac{w^2}{r_i^2} \right) \ln \frac{8r_i}{w} - \frac{1}{2} - 0.0031\frac{w^2}{r_i^2} \right] \tag{11}$$

From the point of view of practical accuracy, quadratic terms in Eq. (11) may be neglected.

Inter-turn mutual inductance M_{ij} is computed with a well-known Maxwell formula [12]:

$$M_{ij} = \mu_0 (r_i + r_j) \left[\left(1 - \frac{k_{ij}^2}{2} \right) K(k_{ij}) - E(k_{ij}) \right], \; i \neq j \tag{12}$$

in which

$$k_{ij} = \frac{2\sqrt{r_i r_j}}{r_i + r_j} \tag{13}$$

and K and E - are the Legendre elliptic integrals:

$$K(x) = \int_0^{\pi/2} \frac{d\theta}{\sqrt{1 - x^2 \sin^2 \theta}} \quad E(x) = \int_0^{\pi/2} \sqrt{1 - x^2 \sin^2 \theta}\, d\theta \tag{14}$$

Mutual inductance between the upper and lower coils M_{12} is computed according to the same principle as the second sum in Eq. (5), with

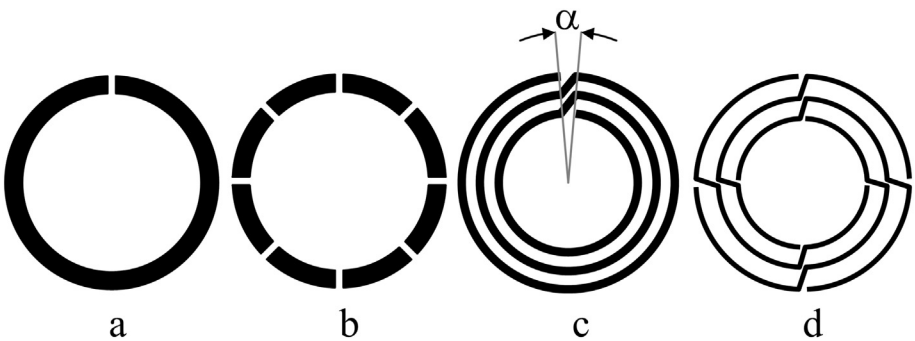

Fig. 4. The types of TLRs (front conductor). (a) Single-turn single-gap (STSG). (b) Single-turn multi-gap (STMG). (c) Mutli-turn single-gap (MTSG). (d) Mutli-turn multi-gap (MTMG). α – the so called an open angle.

the only difference being that now, it is necessary to take into account mutual inductance of turns placed one over another. Therefore, it is necessary to sum over the entire upper triangle of the matrix of inter-turn inductances M_{pq}, including diagonal elements.

$$M_{12} = \sum_{p=1}^{N}\left(\sum_{k\geq p}^{N} M_{pk}\right) M_{pk} = \mu_0\sqrt{(r_p + r_k)^2 + h^2}\left[\left(1 - \frac{m_{pk}^2}{2}\right)K(m_{pk}) - E(m_{pk})\right] \tag{15}$$

in which

$$m_{pk} = \frac{2\sqrt{r_p r_k}}{\sqrt{(r_p + r_k)^2 + h^2}} \tag{16}$$

and K and E - are the Legendre elliptic integrals as it was indicated above.

Another important thing to note is the computation of the coil length l. There is some ambiguity about whether l should be taken as the length of the coil on just one side or both sides. In this paper, l is used as the length of one side of the coil and computed with the following formulas:

With N turns of radii r_i the length of the line is equal to:

$$l = 2\pi\left(1 - \frac{\alpha}{360°}\right)\sum_{i=1}^{N} r_i + \sum_{i=1}^{N-1}\sqrt{r_i^2 + r_{i+1}^2 - 2r_i r_{i+1}\cos\alpha}\,, \text{ for coil in Fig. 4c} \tag{17a}$$

and

$$l = 2\pi\sum_{i=1}^{N} r_i - N\,n\,w_g + n(N-1)\sqrt{(w + w_l)^2 + w_g^2}\,, \text{ for coil in Fig. 4d} \tag{17b}$$

where N is the number of turns of radii r_i, n – the number of gaps in the turns, α – the open angle, as indicated in Fig. 4c, w – the width of the conducting strips, w_l – the width of the spaces between the turns and w_g – the width of the gaps in the strips. It should be noted, that the radii r_i mentioned in the formulas are the outer radii of each turn.

3. Material and methods

All mathematical computations were performed using a custom program coded in MatLab R2016a (Mathworks, Natick, USA). The resonance frequency was computed according to the formulas presented in Section 2.3 by plotting the following function

$$F(\omega_0) = \frac{\omega_0 L}{4nZ_0}\cdot\tan\frac{\omega_0 l\sqrt{\varepsilon}}{4nc} \tag{18}$$

and locating the value closest to 1 and its corresponding $f_0 = \omega_0/2\pi$.

For this paper, twelve TLRs with different configurations were ordered from the company «SEPcoRus» (St. Petersburg, Russia). The coils differed by the following parameters: outer diameter ∅, number of turns N, number of gaps n, width of the conducting strips w, width of the spaces between the turns w_l, open angle α, width of the gaps in the strips w_g, dielectric permittivity ε, thickness of the dielectric h. The main specifications of the TLRs are shown in Table 1. The photograph of the experimental coils is presented in Fig. 5.

To prove the correctness of the formulas presented in this paper, we estimated the uncertainties for the calculated and measured frequencies.

For this each TLR was photographed together with a metal ruler (GOST 427-75 – Russian Federation national standard) using a high-resolution Nikon D3500 digital camera. The mean values and the tolerance of all geometric parameters of the TLRs were determined from the photos in the program ImageJ [13]. The measured parameters were: turn radii r_i, width of the conducting strips w, width of the spaces between the turns w_l, width of the gaps in the strips w_g, open angle α. Results were processed with the aid of the GUM Workbench program [14] and the formula (19) to estimate the type of measured value distributions:

$$V = \frac{N_V\cdot S}{N_S} \tag{19}$$

where V is the measured value, N_V – the distance of the measured value in the image, S – the known length (for example, 10 mm), N_S – the distance in the image corresponding to the known length S. For r_i the normal distribution was proposed. For w, w_l, w_g and α, the trapezoidal [0.3] distribution was suggested.

The calculations also took into account the dielectric permittivity ε and thickness of the dielectric h. For all TLRs, the manufacturing tolerance (0.02) was chosen as the tolerance for ε. The thickness of the dielectric was measured using a digital micrometer Micromar Mahr 40 EWR with the accuracy of 0.002 mm. For ε and h, as no additional information was given, the distribution was proposed as uniform.

Due to the high complexity of the computational uncertainty calculation by the analytical method, the simulation for the resonance frequency was carried out using the Monte Carlo method according to the recommendations of JCGM 101: 2008 [15]. To do this, 10,000 values for each measured parameter were generated with a proposed distribution type, mean value and tolerances. Then, the resonance frequency was computed for each set of value. The results of the calculations were plotted as a histogram and fitted by a normal distribution. The expanded uncertainty of the calculated frequency with 95% coverage was determined as the standard deviation of the simulated distribution multiplied by the coverage factor k for the normal distribution ($k = 2$).

The calculation of the experimental uncertainty was performed using the following formula (20):

$$u(f_{meas}) = k\sqrt{u_A^2(f_{meas}) + u_B^2(f_{meas})} \tag{20}$$

where k is a coverage factor, $u_A(f_{meas})$ – type A uncertainty, $u_B(f_{meas})$ – type B uncertainty. In our case k equals 2, because it was found that the measured value has normal distribution (as a result of Monte Carlo simulation according to the following model: $f = f_{meas} + df$, where f_{meas} is the measured frequency, df – the tolerance of the measured frequency).

To calculate the $u_A(f_{meas})$ for each TLR we made 10 measurements of the resonance frequency using a Network Analyzer Rohde & Schwarz ZVH4 1309.6800.24 by means of a single-probe loop method [16]. Then, type A uncertainty was calculated using the following formula (21):

$$u_A = \sqrt{\frac{1}{N(N-1)}\sum_{i=1}^{N}(N_i - N_{mean})^2} \tag{21}$$

where N is the number of measurements (Eq. (10)), N_i – the value of the i-th measurement, N_{mean} – the mean value of all measurements for the one coil.

Type B uncertainty was estimated from the manufacturer's specification for the Network Analyzer. According to the specification, the accuracy of the frequency reading was calculated by the following formula (22):

$$\Delta f\,[Hz] = \pm\left(f_0\cdot\Delta f_{rel} + 0.1\cdot b_{meas} + 0.5\cdot\frac{f_{stop} - f_{start}}{p-1} + 1\right) \tag{22}$$

where f_0 is the marker frequency (measured frequency, MHz), Δf_{rel} – the reference accuracy ($1\cdot10^{-6}$), b_{meas} – the measurement bandwidth (10 kHz), f_{start} and f_{stop} – the beginning and the end of the measurement range (20 MHz), respectively, p – the data points (201).

We assumed that these limits cover at least 95% of the normally distributed measured value. So, the recalculation of the measurement accuracy into the experimental uncertainty was performed by the use of

Table 1
Specifications of coils and results.

Geometrical parameters								Dielectric		Resonance frequency f_0 (MHz)		
№	N	n	∅ (mm)	w (mm)	w_l (mm)	w_g (mm)	α (deg)	ε	h (mm)	Computation	Measurement	Deviation (%)
1	6	6	50	1.64 ± 0.10	1.03 ± 0.06	4.00 ± 0.10	–	2.20 ± 0.02	0.960 ± 0.002	262.69 ± 5.48	263.14 ± 0.09	−0.17
2	6	6	50	1.60 ± 0.10	1.38 ± 0.08	4.00 ± 0.10	–	2.20 ± 0.02	0.960 ± 0.002	282.15 ± 5.24	283.09 ± 0.09	−0.33
3	5	4	40	1.34 ± 0.08	1.10 ± 0.06	3.00 ± 0.10	–	2.20 ± 0.02	0.960 ± 0.002	290.92 ± 5.04	286.14 ± 0.09	+1.64
4	5	4	40	1.28 ± 0.08	1.54 ± 0.08	3.00 ± 0.10	–	2.20 ± 0.02	0.960 ± 0.002	318.21 ± 5.60	314.48 ± 0.09	+1.17
5	4	2	30	1.32 ± 0.08	0.88 ± 0.06	2.00 ± 0.10	–	2.20 ± 0.02	0.960 ± 0.002	259.63 ± 4.90	258.75 ± 0.09	+0.34
6	4	2	30	1.34 ± 0.08	1.18 ± 0.05	2.00 ± 0.10	–	2.20 ± 0.02	0.960 ± 0.002	275.65 ± 5.16	278.02 ± 0.09	−0.86
7	3	1	20	1.01 ± 0.06	0.63 ± 0.05	–	15.0 ± 0.3	2.20 ± 0.02	0.960 ± 0.002	290.74 ± 7.32	295.16 ± 0.09	−1.52
8	3	1	20	1.00 ± 0.06	0.80 ± 0.06	–	15.0 ± 0.3	2.20 ± 0.02	0.960 ± 0.002	301.84 ± 7.26	306.24 ± 0.09	−1.46
9	5	6	30	1.06 ± 0.06	0.54 ± 0.05	2.00 ± 0.10	–	2.20 ± 0.02	0.125 ± 0.002	259.42 ± 6.48	257.80 ± 0.09	+0.62
10	5	6	30	1.03 ± 0.06	0.76 ± 0.06	2.00 ± 0.10	–	2.20 ± 0.02	0.125 ± 0.002	275.81 ± 6.96	276.72 ± 0.09	−0.33
11	6	4	20	0.62 ± 0.05	0.60 ± 0.05	1.50 ± 0.10	–	2.20 ± 0.02	0.125 ± 0.002	307.39 ± 9.86	299.44 ± 0.09	+2.59
12	6	2	10	0.16 ± 0.04	0.22 ± 0.04	0.50 ± 0.10	–	2.20 ± 0.02	0.125 ± 0.002	394.37 ± 26.96	386.16 ± 0.09	+2.08

formula (23) in accordance with GUM recommendations [15]:

$$u_B(f_{meas}) = \frac{\Delta f}{1.98} \tag{23}$$

4. Results

Verification of the proposed algorithm was conducted, comparing computed data with the experimental measurements. Specifications of the obtained values are presented in Table 1 along with computational and experimental results. Fig. 6 presents a graph showing the overlap of the calculated and measured frequencies for each coil.

As shown in Table 1, the resonance frequencies computed using the method outlined in this paper are in very good agreement with experimental results. Note that a rather large computational uncertainty was obtained only for TLR №12. For this coil, the width of the conducting strips w and the width of the spaces between the turns w_l are too small to be reliably measured using our equipment. As a result, the tolerance for w was 25%, and for w_l – 18%, what was the result of increasing the uncertainty.

The deviations of the computed values from the measured values are less than 3%, which is a good result. Such deviations may be

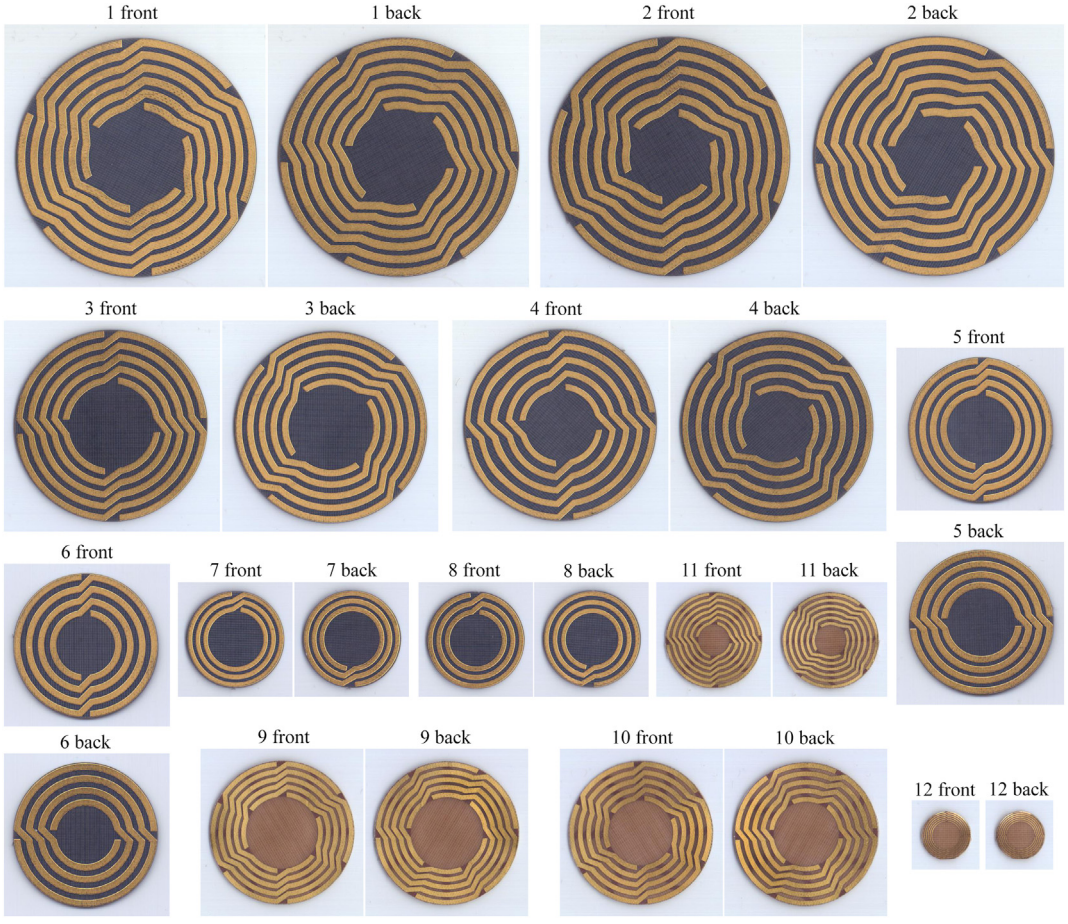

Fig. 5. Photograph of the experimental TLRs. All coils are on the same scale.

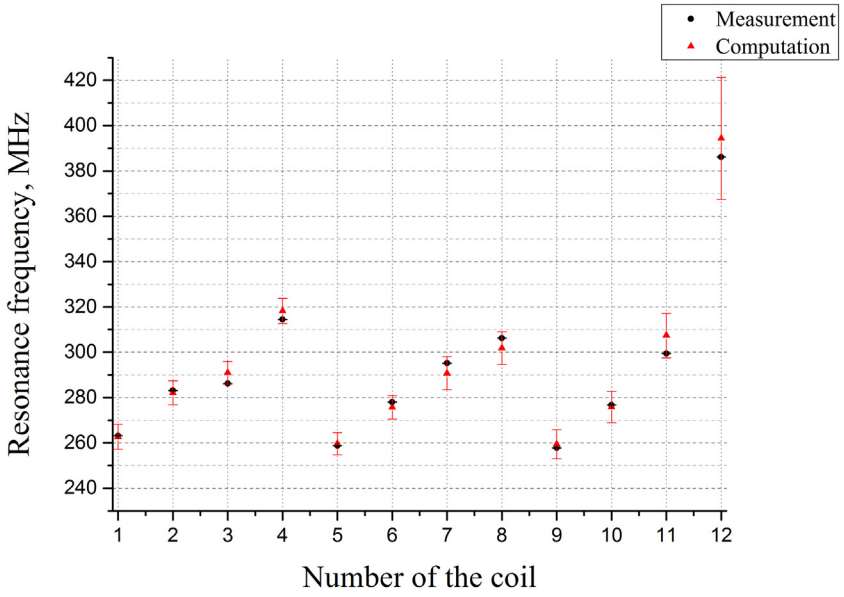

Fig. 6. The computational and experimental frequencies for each coil.

attributed to the approximate nature of the impedance formula, meaning that the computed value will be slightly below the real one, which results in the resonance frequency being underestimated. This, however, seems to have only a marginal effect on the deviation of the resonance frequency, since the experiment clearly shows both positive and negative deviations.

It was of interest to compare the results obtained using our correction formulas with the ones presented in literature, for example in the paper of Megherbi et al. [7]. In this work, the resonance frequencies f_0 were computed for the five-turn circular coil with one gap, with the outer diameter ∅ = 14.6 mm, various strip widths w, width of the spaces between the turns w_l = 0.3 mm and various thicknesses h and dielectric permittivity ε. In Figs. 7 and 8 the dependency graphs of the resonance frequency of the mentioned above coil on the dielectric permittivity ε and the width of the conducting strips w, respectively, obtained by Megherbi et al. [7] and by using the proposed technique are presented.

Analysis of these results shows a good agreement between the results presented in the current work and by Megherbi et al. [7].

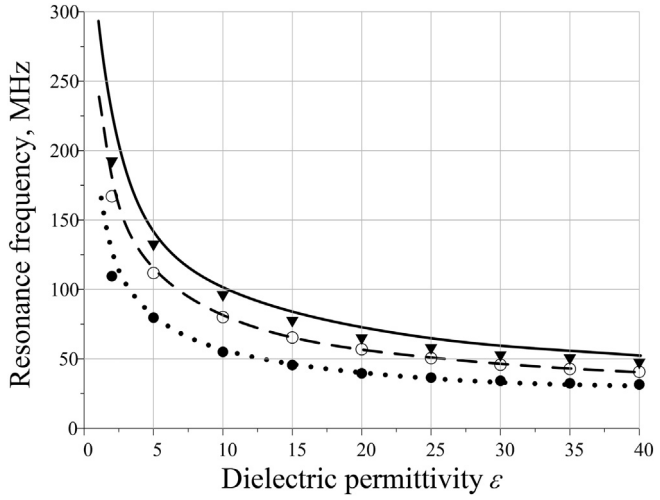

Fig. 7. Resonance frequency as a function of dielectric permittivity ε with w = 0.4 mm. Lines - results from Megherbi et al. [7], dots - computations according to the proposed technique. Solid line: h = 0.5 mm; dashed line: h = 0.25 mm; dotted line: h = 0.1 mm. The proposed technique gave the results shown by triangles, open and solid circles, respectively.

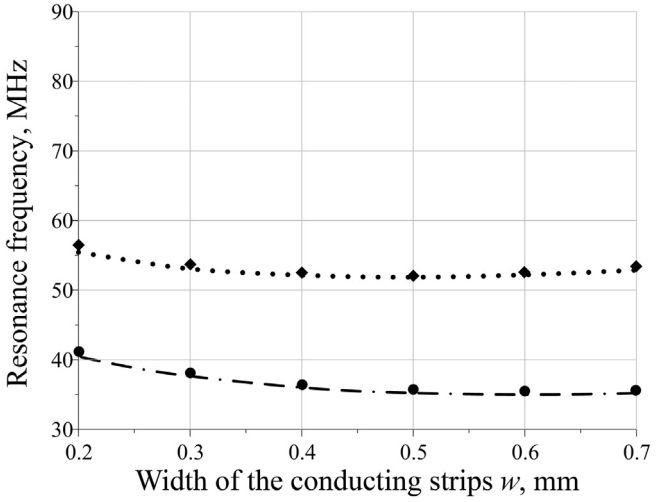

Fig. 8. Resonance frequency as a function of the strip width w with ε = 23.6. Lines - results from Megherbi et al. [7], dots - computations according to the proposed technique. Dotted line: h = 0.25 mm; dash-dotted line: h = 0.1 mm. The proposed technique gave the results shown by rhomboids and solid circles, respectively.

Another work with which we compared the use of our correction formulas for computation of the resonance frequency is the paper of Serfaty et al. [5]. By specifying the outer diameter ∅, the number of turns N, the number of gaps n, the width of the conducting strips w, the width of the spaces between the turns w_l, the dielectric permittivity ε and the thickness of the dielectric h, we computed the resonance frequency of the TLRs and compared the values of f_0 with the ones obtained in his work. In Table 2, the corresponding specifications of the coils and results are presented.

As shown in Table 2, the resonance frequencies of the TLRs computed using our correction formulas coincide with the ones measured by Serfaty et al. [6] within the margin of error (up to 3%). Only for coil number 5, the values of f_0 are very different. This may be because one of the parameters of this coil presented in Table 1 in the paper of Serfaty et al. [6] has a typo. This may also be indicated by deviations obtained for all TLRs made specifically for this work, which were no more than

Table 2
Specifications of the coils from the paper of Serfaty et al. [5] and results.

Geometrical parameters[a]						Dielectric[a]		Resonance frequency f_0 (MHz)			
№	N	n	w (mm)	w_l (mm)	∅ (mm)	ε	h (mm)	Computation[a]	Proposed technique	Measurement[a]	Deviation[a] (%)/deviation (%)
1	2	1	10	1	163	4.1	0.61	11.16	11.76	11.46	−2.7/+2.5
2	3	1	10	1	163	4.1	0.61	7.28	7.68	7.44	−2.2/+3.1
3	4	1	10	1	163	4.1	0.61	5.65	5.88	5.79	−2.5/+1.5
4	4	1	11	0.65	163	4.1	1.55	8.90	9.08	9.14	−2.7/−0.7
5	6	1	4	0.50	134	4.1	1.55	7.43	8.31	7.23	+2.8/+13.0

[a] This data was taken from the paper of Serfaty et al. [5].

3%.

It should also be noted that our formulas give overestimated values of the resonance frequencies in comparison with the ones computed by Serfaty et al. [6]. Such deviations may be explained by subtle differences in the methods used to compute the frequencies. For instance, the formula for computing the impedance Z_0 was taken from the paper of Grover et al. [17], which is different from formulas (2) and (3) used in the current work. Nevertheless, the small magnitude of these deviations indicates that both methods are valid for the purpose of obtaining the resonance frequencies of TLRs.

Note that the coils presented in this work are meant to be implanted into the studied tissue. This means, that in order to reduce the effects of implant rejection they are coated in a silicon-based compound, which, according to previous studies [18], tends to reduce the resonance frequency by approximately 8%, which is several times larger than the deviations observed in the experiment. This means that while the deviations between the computed and measured resonance frequencies are regrettable, they are significantly smaller than the deviations caused by other factors. Therefore, the proposed technique for computing resonance frequency of the TLRs is indeed practical.

5. Conclusion

For the first time, fundamental mistakes in formulas for computing resonance frequency of the TLRs used in MRI, which can be found in the literature, are summarized and analyzed. Corrected formulas are presented and a numeric technique for computations is outlined.

Acknowledgements

We thank Dmitry Frolov for the help in estimating the uncertainties for the calculated and measured frequencies. This work was supported by Russian Science Foundation Grant no. 17-79-10448.

Appendix A

Computation of the limit of R when $b \to 0$. Firstly, resolve indeterminate forms. At small b in Eq. (9) use the Maclaurin series of the first order for the components:

$$\ln\sqrt{1+\frac{b^2}{a^2}} \approx \frac{1}{2}\frac{b}{a}\operatorname{arctg}\frac{b}{a} \approx \frac{b}{a} \tag{A.1}$$

Indeterminate form of the type $x\ln\left(\frac{1}{x}\right)$ at $x \to 0$ tends to zero, because the logarithm always changes slower than x. The rest of the terms in Eq. (9) are all of determinate forms at $b \to 0$: $arctg(\infty) = \pi/2$. We have then:

$$\ln R \approx \ln a - \frac{1}{12} + \frac{2}{3} + \frac{\pi}{3}\frac{b}{a} - \frac{25}{12} \to \ln a - \frac{3}{2} \tag{A.2}$$

And eventually:

$$R = a \cdot e^{-3/2} \approx 0.223a \tag{A.3}$$

References

[1] Hoult DI, Richards RE. The signal-to-noise ratio of the nuclear magnetic resonance experiment. J Magn Reson 1976;24(1):71–85. https://doi.org/10.1016/0022-2364(76)90233-X.
[2] Zabel HJ, Bader R, Gehrig J, Lorenz WJ. High-quality MR imaging with flexible transmission line resonators. Radiology 1987;165(3):857–9. https://doi.org/10.1148/radiology.165.3.3685365.
[3] Gonord P, Kan S, Leroy-Willig A. Parallel-plate split-conductor surface coil: analysis and design. Magn Reson Med 1988;6(3):353–8. https://doi.org/10.1002/mrm.1910060313.
[4] Gonord P, Kan S, Leroy-Willig A, Wary C. Multigap parallel-plate bracelet resonator frequency determination and applications. Rev Sci Instrum 1994;65(11):3363–6. https://doi.org/10.1063/1.1144573.
[5] Serfaty S, Haziza N, Darrasse L, Kan S. Multi-turn split-conductor transmission-line resonators. Magn Reson Med 1997;38(4):687–9. https://doi.org/10.1002/mrm.1910380424.
[6] Frass-Kriegl R, Laistler E, Hosseinnezhadian S, Schmid AI, Moser E, Poirier-Quinot M, et al. Multi-turn multi-gap transmission line resonators – concept, design and first implementation at 4.7 T and 7 T. J Magn Reson 2016;273:65–72. https://doi.org/10.1016/j.jmr.2016.10.008.
[7] Megherbi S, Ginefri JC, Darrasse L, Raynaud G, Pone JF. Behavioral VHDL-AMS model and experimental validation of a nuclear magnetic resonance sensor. Microsyst Technol 2005;12:38–43. https://doi.org/10.1007/s00542-005-0068-9.
[8] Teng Q. Structural biology: practical NMR applications. 2nd ed. New York: Springer; 2013. https://doi.org/10.1007/978-1-4614-3964-6.
[9] Wheeler HA. Transmission-line properties of parallel strips separated by a dielectric sheet. IEEE Trans Microwave Theory Tech 1965;13(2):172–85. https://doi.org/10.1109/TMTT.1965.1125962.
[10] Rosa EB, Grover FW. Formulas and tables for calculation of mutual and self-inductance. Scientific papers of the bureau of standards. 3rd ed. Washington: Govt. Print. Off; 1916.
[11] Rosa EB. Calculation of the self-inductance of single-layer coils. Bull Bur Stan 1906;2(2):161–87.
[12] Smythe WR. Static and dynamic electricity. 2nd ed. New York: McGraw-Hill Book Company Inc; 1950. [Ch.8, §8.06, art (1)].
[13] Abramoff MD, Magalhaes PJ, Ram SJ. Image processing with ImageJ. J Biophotonics Int 2004;11(7):36–42.
[14] GUM workbench educational version. http://www.metrodata.de/download_en.html, Accessed date: 30 April 2019.
[15] BIPM, IEC, IFCC, ILAC, ISO, IUPAC, et al. Evaluation of measurement data –

supplement 1 to the «guide to the expression of uncertainty in measurement» – propagation of distributions using a Monte Carlo method. Joint Committee for Guides in Metrology, Bureau International des Poids et Mesures; 2008https://www.bipm.org/utils/common/documents/jcgm/JCGM_101_2008_E.pdf, Accessed date: 30 April 2019.

[16] Ginefri JC, Durand E, Darrasse L. Quick measurement of nuclear magnetic resonance coil sensitivity with a single-loop probe. Rev Sci Instrum 1999;70(12):4730–1. https://doi.org/10.1063/1.1150142.

[17] Grover FW. The calculation of the mutual inductance of circular filaments in any desired positions. Proc IRE 1944;32(10):620–9. https://doi.org/10.1109/JRPROC.1944.233364.

[18] Ginefri JC, Rubin A, Tatoulian M, Woytasik M, Boumezbeur F, Djemai B, et al. Implanted, inductively-coupled, radiofrequency coils fabricated on flexible polymeric material: application to in vivo rat brain MRI at 7T. J Magn Reson 2012;224:61–70. https://doi.org/10.1016/j.jmr.2012.09.003.